Environ. Sci. Technol. **2004**, *38,* 4656−4663

In Situ Chemical Reduction of Aquifer Sediments: Enhancement of Reactive Iron Phases and TCE Dechlorination

JIM E. SZECSODY,* JONATHAN S. FRUCHTER, MARK D. WILLIAMS, VINCE R. VERMEUL, AND DEBBIE SKLAREW

Pacific Northwest National Laboratory, Richland, Washington 99352

In situ chemical reduction of aquifer sediments is currently being used for chromate and TCE remediation by forming a permeable reactive barrier. The chemical and physical processes that occur during abiotic reduction of natural sediments during flow by sodium dithionite were investigated. In different aquifer sediments, 10−22% of amorphous and crystalline Fe^{III}-oxides were dissolved/reduced, which produced primarily adsorbed Fe^{II}, and some siderite. Sediment oxidation showed predominantly one Fe^{II} phase, with a second phase being oxidized more slowly. The sediment reduction rate (3.3 h batch half-life) was chemically controlled (58 kJ mol^{-1}), with some additional diffusion control during reduction in sediment columns (8.0 h half-life). It was necessary to maintain neutral to high pH to maintain reduction efficiency and prevent iron mobilization, as reduction generated H^+. Sequential extractions on reduced sediment showed that adsorbed ferrous iron controlled TCE reactivity. The mass and rate of field-scale reduction of aquifer sediments were generally predicted with laboratory data using a single reduction reaction.

Introduction

Iron oxides are ubiquitous in the subsurface environment and, because they can be chemically and biotically reduced, may represent an efficient means to create in situ redox-reactive barriers at great depth. Groundwater remediation using permeable reactive barriers or wells (*1*) has been found to offer the significant economic advantage of in situ treatment while relying upon chemical technologies proven in industrial settings (*2*). Once a redox-reactive barrier is in place, mobile contaminants in groundwater are reduced/precipitated or degraded for decades with no additional manipulation. Reactive barriers for reduction of metals (*3*−*5*), dechlorination of organic solvents (*6, 7*), and reduction of nitroaromatics (*8, 9*) are being implemented using primarily zerovalent iron (*10, 11*), iron−Cr (*12*), and, in a few cases, by reduction of natural sediments (*13, 14*). This laboratory study investigates geochemical changes that occur during chemical reduction of natural sediments and identifies which surface phases subsequently dechlorinate TCE (*15, 16*).

Natural sediments that have been chemically reduced with sodium dithionite have been tested on organic solvents [1,1-dichloroethylene (1,1-DCE), trichloroethylene (TCE), tetrachloroethylene (PCE)], metals (Cr, U, Tc), and explosives [2,4,6-trinitrotoluene (TNT), hexahydro-1,3,5-trinitro-1,3,5-triazine (RDX), hexanitrohexaazaisowurtzitane (CL-20), *N*-nitrosodimethylamine (NDMA)]. Chemical reduction of clays has shown that structural ferrous iron dechlorinates aliphatic compounds (*16, 17*). Although reduction of some metals is rapid (Cr) and some can be reduced by aqueous Fe^{II}, the slow reduction of chlorinated compounds by reduced sediment and Fe^0 requires both Fe^{II} as an electron donor and a clay or iron oxide (*18, 19*), or Fe^0 surface (*20*). Because natural sediments have a low (<3%) iron oxide content relative to Fe^0, surface conditions necessary for solvent dechlorination may not occur in some cases. Clearly, a better understanding is needed of the iron surface phases present in chemically reduced sediment that are reacting with contaminants.

Moreover, successful application of a reactive barrier technology in the subsurface requires an understanding of the geochemical and hydraulic aspects of the barrier, so a comparison here is made between zerovalent and reduced sediment barriers. For zerovalent iron, the surface may act as a catalyst or a semiconductor, or provide the necessary surface coordination for the electron-transfer reactions (*21, 22*). The electron donor may be the zerovalent iron (*23*), although there is an increase in reaction efficiency upon initial Fe^{II} oxide formation on surfaces. At longer times, the buildup of Fe^{III} oxyhydroxides occurs (*24*), which dramatically decreases reduction efficiency. Although permeable Fe^0 barriers have significant electron donor capacity, some of the loss in barrier reactivity (*25, 26*) is caused by physical and other secondary effects. The passivation of iron surfaces is caused by precipitation of metal oxides/hydroxides of contaminants and other aqueous ions present (*24, 27*), which have a greater impact on the upgradient portion of the thin Fe^0 walls. Significant precipitate can decrease permeability as much as an order of magnitude (*28*), resulting in a less efficient reactive barrier. In addition, high conductivity zones intersecting thin Fe^0 barriers can cause barrier failure (*29*). The impact of these physical processes may be less on reduced natural sediments since precipitates would be more spread out with the low iron content of reduced natural sediments. Therefore, in situ dithionite reduction of sediments may offer some hydraulic advantages over Fe^0 barriers but reduced sediment may not be as reactive.

Dithionite treatment reduces structural iron in clays (*17, 30*), dissolves and reduces amorphous and some crystalline Fe^{III} oxides (*31*), so may react with both iron oxides and clays in natural sediments, producing mainly one or more Fe^{II} species (*15*). This occurs by the initial rapid dissociation of dithionite in aqueous solution, followed by reduction of ferric iron phases

$$S_2O_4^{2-} \leftrightarrow 2SO_2^{\bullet-} \quad (1)$$

$$SO_2^{\bullet-} + Fe^{3+} + H_2O \leftrightarrow Fe^{\bullet 2+} + SO_3^{2-} + 2H^+ \quad (2)$$

Because Fe^{II} at mid- to high-pH low-ionic-strength groundwater has a high affinity for Fe^{III} oxide surfaces, Fe^{II} is not mobilized. The four moles of H^+ produced per mole of dithionite consumed are neutralized by a carbonate buffer. The presence of dithionite in aqueous solution will slowly disproportionate at a rate ~5 times slower than iron reduction (*19*)

$$2S_2O_4^{2-} + H_2O \leftrightarrow S_2O_3^{2-} + 2HSO_3^- \quad (3)$$

* Corresponding author phone: (509) 372-6080; fax: (509) 375-6954; e-mail: jim.szecsody@pnl.gov.

10.1021/es034756k CCC: $27.50
Published on Web 07/29/2004

TABLE 1. Iron Extractions of Untreated and Treated Sediment Samples[a]

			Fe^{II}				Fe^{III}				$Fe^{II} + Fe^{III}$
					total				total		
sed.	exp.	treatment	CO_3/S	sorbed		%[b]	am.	cryst.		%[b]	total
#1		untreated	17.8	0.24	51.8	*8.3*	85.7	106	573	*91.7*	625
	B	reduced, 0−5 cm	35.9	155	60.5	*30.5*	47.6		465	*74.4*	525
	B	reduced, 5−10 cm	62.3	77.4		*22.3*		116			
	B	reduced, 10−15 cm	54.7	82.0	83.4	*21.9*	45.4		493	*78.9*	576
	C	reduced, oxidized	27.7	0.03	56.9	*9.1*	75.0	150	475	*76.0*	532
	D	reduced, oxidized	33.9		64.8	*10.4*	69.6		527	*84.3*	592
#2		untreated	12.8	0.0	36.6	*24.6*	37.9	46.5	113	*75.8*	149
	H	reduced	18.5	29.8	56.5	*37.9*	24.1	40.8	101	*67.8*	158
#3		untreated	28.5	0.0	62.3	*9.2*	188	284	611	*90.6*	674
	N	reduced	31.9	98.5	70.9	*19.3*	93.2	119	626	*92.9*	697
	O	reduced, oxidized	111	0.08	61.5	*16.5*	127		543	*80.6*	604
#4		untreated	11.4	0.0	24.4	*35.6*	11.6	12.7	44.1	*64.4*	68.5
		reduced	24.1	7.7	31.8	*46.4*	5.7	9.8	33.5	*48.9*	65.4
	Q	reduced, oxidized	17.1	0.0	20.3	*29.6*	23.0	13.0	46.6	*68.0*	66.8

[a] Chemical extractions all in μmol g^{-1} except % in italics. $FeCO_3$+FeS = 0.5 M HCl − 1 M $CaCl_2$, ads. Fe^{II} = 1 M $CaCl_2$; total Fe^{II} = 5 M HCl (% in italics). Am.-Fe^{III} oxides = NH_2OH·HCl, cryst. Fe^{III} oxides = DCB − NH_2OH·HCl; total Fe^{III} = 5 M HCl (% in italics). Fe^{II} + Fe^{III} total = total Fe^{II} + total Fe^{III}. [b] Percent of untreated sediment total Fe^{II} + Fe^{III}.

and so dithionite is unavailable for iron reduction at large contact times. The longevity of a reduced sediment barrier is dependent on the flux of electron acceptors into the reduced zone (dissolved oxygen, chromate, TCE, nitrate, uranium (*15*)). In relatively uncontaminated aquifers, dissolved oxygen in water is the dominant oxidant. Although the rate of oxidation of aqueous Fe^{II} by oxygen at pH 8 has a 2−3-min half-life (*2*, *32*), slower rates are likely for the oxidation of surface Fe^{II} phases. The oxidation rate of the barrier significantly influences the barrier design, as contaminants need to be reduced/degraded within the limited residence time within the reduced zone.

The purpose of this study is to quantify reactive phases that result from in situ reduction of natural sediments and determine which reactive phases control TCE redox reactivity. It is hypothesized that the reductive dissolution of several Fe^{III} phases in natural sediments by dithionite contribute to the rate of sediment reduction. Reduction and oxidation experiments with natural sediments over a range of reactant concentration, pH, and temperature conditions were used to identify chemical and physical changes. While dominant reactive phases have been clearly identified with reduction of minerals (*6*, *18*), reduction of natural sediments results in multiple reactive surface Fe^{II} phases. We physically and chemically separated different iron-containing components of reduced natural sediment to determine the redox reactivity of TCE, which requires both an electron donor and a surface catalyst for dechlorination (*18*, *19*). We hypothesize that adsorbed Fe^{II} on clays dominates TCE dechlorination in chemically reduced natural sediments. The findings of this experimental study provide insights into the chemical characterization and reduction rates expected at the field scale and the expected longevity of redox reactive permeable zones created by in situ chemical reduction of natural sediments.

Materials and Methods

Materials. Experiments were conducted on aquifer sediments from differing geologic environments to quantify iron phase changes due to dithionite treatment. The two silty gravel sediments (#1 glacial and #2 fluvial in Table 1) are from aquifers (60 ft and 40 ft depth) in Tacoma and Vancouver, Washington. The silty sand (#3 estuarine) is from a confined aquifer (65 ft depth) in Palo Alto, California, and the sandy gravel (#4, fluvial) is from an unconfined aquifer (95 ft depth) on the Hanford Site in Eastern Washington. Sediment #1 had 2.8 ± 0.8% clay (<2 μm), in which X-ray diffraction indicated chlorite, vermiculite, and smectite. Sieve and hydrometer analysis of sediment #1 showed that the <30 μm size fraction (used in some TCE experiments) was 82% clay (<2 μm). The subsurface sediments were treated with a laboratory grade 10^{-3} to 10^{-1} mol L^{-1} sodium dithionite (sodium hydrosulfite; CAS 7775-14-6), 10^{-3} to 4×10^{-1} mol L^{-1} K_2CO_3, and 10^{-4} to 10^{-2} mol L^{-1} $KHCO_3$. Iron extractions conducted on untreated, reduced, and reduced/oxidized sediments from 1-D columns (Table 1) in an anaerobic chamber consisted of (a) 1 M $CaCl_2$ (Fe^{II} ion exchangeable) (*33*), (b) 0.5 M HCl (*33*), (c) NH_2OH, HCl (*34*), (d) dithionite−citrate−bicarbonate (DCB) (*33*), and (e) 5 M HCl (*33*). Each extraction was conducted in triplicate (standard deviations were ±3.3−8.3%), with additional duplication for some samples. In some cases, a portion of sediment from a column experiment was analyzed (i.e., 0−5 cm of a 15-cm column). Aqueous Fe^{II} and Fe_{total} from extractions were quantified by ferrozine (*35*), where Fe_{total} (Fe^{II} + Fe^{III}) samples reduced aqueous Fe^{III} to Fe^{II} by 0.025 M NH_2OH, HCl. Extracted Fe^{III} was the difference between Fe_{total} and Fe^{II}. The $FeCO_3$/FeS phase was defined by the 0.5 M HCl minus the 1 M $CaCl_2$ extraction. Amorphous and poorly crystalline Fe^{III} oxides were defined by the NH_2OH, HCl extraction, and crystalline Fe^{III} oxides were defined by the DCB minus the NH_2OH, HCl extraction (*33*). Total Fe^{II} and Fe^{III} oxides and carbonates were defined by the 5 M HCl extraction. Ethylene glycol monoethyl ether was used to measure total surface area (duplicate samples, ±8%).

Sediment Reduction and Oxidation Experiments. Batch experiments consisted of a single large septa-top glass bottle in which 14−200 g of sediment was reacted with 500 mL of dithionite solution for hundreds of hours on a slow linear shaker in a temperature-controlled chamber (2−42 °C). Of 14 experiments, 3 were duplicates. Dithionite solutions were prepared in anaerobic chambers additionally bubbling He for 30 min in the solution before adding dithionite. At specific time intervals, a sample was withdrawn, filtered, and analyzed for dithionite remaining in solution. Column reduction studies consisted of injecting the dithionite solution into a 15-cm-long sediment column and measuring the effluent dithionite concentration to determine the loss due to iron reduction. The flux rate was chosen to achieve specific residence times of the dithionite solution in the column (2−

TABLE 2. Sediment Reductive Capacity with Dithionite Treatment

sed.	exp.	residence time (h)[a]	K_2CO_3[b] (mol L^{-1})	reduction half-life (h)	Fe^{II} reduced (μmol g^{-1})	Fe^{III} oxidized (μmol g^{-1})
#1	A	2.6	0.36	5.84	149	159
	B	2.9	0.36		137	141
	C	2.5	0.36	5.21	129	137
	D	3.3	0.36	4.87	142	132
	E	2.2	0.27	4.53	85.1	79.2
	F	2.2	0.18	6.77	66.0	58.2
	G	2.9	0.045	7.56	37.4	41.5
#2	H	7.9	0.36	6.90	51.4	
	I	7.0	0.36	11.8	46.8	
	J	4.0	0.36	5.08	28.7	32.1
	K	12	0.36	8.56	31.9	28.9
	L	11	0.36	7.93	40.7	41.4
#3	M	1.6	0.36	2.44	557	421
	N	3.3	0.36	3.50	552	
	O	12	0.36	4.94	450	387
#4	P	2.3	0.36	6.54	12.7	8.51
	Q	2.1	0.36	5.12	11.2	9.63
	R	2.7	0.36	5.96	10.9	8.39

[a] For reduction. [b] All with 0.09 mol L^{-1} sodium dithionite.

14 h) to be similar to the reduction half-life (*36*). The mass of reduced iron in dithionite-treated sediments was additionally measured in columns by injecting O_2-saturated water for hundreds to thousands of pore volumes until oxygen consumption ceased. Reductive capacity of sediments is dependent on the oxidizing species (*37*). The dry bulk density and porosity of the column were calculated from the dry and saturated column weight and column volume. The columns were packed with dry sediment in an oxic environment, saturated with water (1.0 mmol L^{-1} $CaCl_2$), weighed, then subjected to dithionite treatment in a sealed system. The volumetric flow rate was calculated from the effluent volume and elapsed time. The electrical conductivity of the column effluent (via flow-through electrode and data-logging) provided a second measure of the porosity. The dithionite concentration was measured using an automated fluid system and data logging equipment with stainless steel components to eliminate any oxidation via diffusion. In this system, a 15−45 μL sample in an HPLC injection valve (Valco Instruments, Houston, TX) was mixed with 10 mL of water using a multi-valve syringe pump (Kloehn, Ltd., Las Vegas, NV), then absorption at 315 nm measured with a flow-through UV detector. Reduction and oxidation experiments were run in triplicate (Table 2) with reducible iron content precision of ±10%.

TCE Experiments. Batch experiments were conducted by reacting the chemically reduced sediment with trichloroethylene (TCE, CAS 79-01-6) to determine the TCE degradation rate of different ferrous surface phases. In some cases, TCE experiments were conducted on chemically reduced sediment, which was additionally treated (iron extractions, previously described) to remove differing Fe^{II} phases. Batch TCE experiments consisted of reacting aqueous TCE with 0.5 g of reduced sediment in 10-mL glass septa-top vials (10-mm-thick septa) with no headspace for times from minutes to 240 h. Of 16 experiments, 3 were duplicates. Vials were placed on low rpm rotary mixers in a temperature-controlled chamber (16 °C). Mixing of the sediment, water, and TCE was accomplished in an anaerobic chamber to minimize the oxidation. At specified times, vials were sacrificed, and 2−5 mL of water was extracted, filtered (0.22 μm Teflon), and injected into 154-mL septa-top glass vials. After 24 h of shaking, 1.0 mL of headspace in the anaerobic vials was analyzed for TCE and degradation products (chloroacetylene, acetylene). Henry's law was used to calculate the total mass originally in the samples. Samples (with 10% duplication) were analyzed by gas chromatography using a flame ionization detector and GS Gaspro column (30 m × 0.32 mm) with 4.6 mL min^{-1} helium flow rate. The initial column temperature was 45 °C; it was programmed at 15 °C min^{-1} to 260 °C, then held isothermal for 5 min. Fluorobenzene was used as an internal standard for TCE; acetylene was calibrated using an external standard.

Modeling. The reductive dissolution and disproportionation reactions that described iron species reduction or oxidation and dithionite species disappearance over time were incorporated into a numerical model to quantify batch and column experimental results. Differential mass flux equations of the species were numerically solved with a stiff reaction solver method (*38*). Reactive transport simulations with reduction or oxidation reaction were solved numerically with a full operator-splitting method. A third-order method with a total variation diminishing (TVD) property was used for the advection subproblem (*39*). Given that more than one Fe^{III} oxide was being reduced, schemes tested included two reductive dissolution reactions (duplicates of reaction 2, different rates). The first-order disproportionation reaction (reaction 3) was incorporated without change. One or two Fe^{II} phase reactions were used to describe sediment oxidation.

Results and Discussion

Iron Phase Changes During Reduction. Dithionite treatment of sediments ("reduced" in Table 1) increased the relative amount of Fe^{II} phases from 10 to 22%, with a corresponding decrease in Fe^{III} phases relative to untreated sediments. The untreated sediments had a 5 M HCl extractable iron content (Fe^{III} + Fe^{II}) that varied from 68 (sediment #4) to 674 μmol g^{-1} (sediment #3). Because all of these sediments were from oxic aquifers, Fe^{III} phases dominated (64−92% of total Fe) compared with Fe^{II} phases (8−36%). The 5 M HCl extraction of reduced sediment #1 was dominated by Fe with only 3.7% Mn (by ICP-MS (*33*)).

Additional iron phase extractions showed that the dithionite treatment increased mainly adsorbed Fe^{II}, with a smaller increase in $FeCO_3$/FeS. For example, sediment #1 reduction (experiment B, Table 1) increased adsorbed Fe^{II} from 0.2 to 155 μmol g^{-1} and increased $FeCO_3$/FeS from 18 to 36 μmol g^{-1}. Dithionite reduction also decreased both amorphous and crystalline Fe^{III} oxides, with amorphous Fe^{III} oxides to a greater extent. Iron extraction data did not fully account for solid-phase iron present, as 30−60% of the total Fe^{III} was

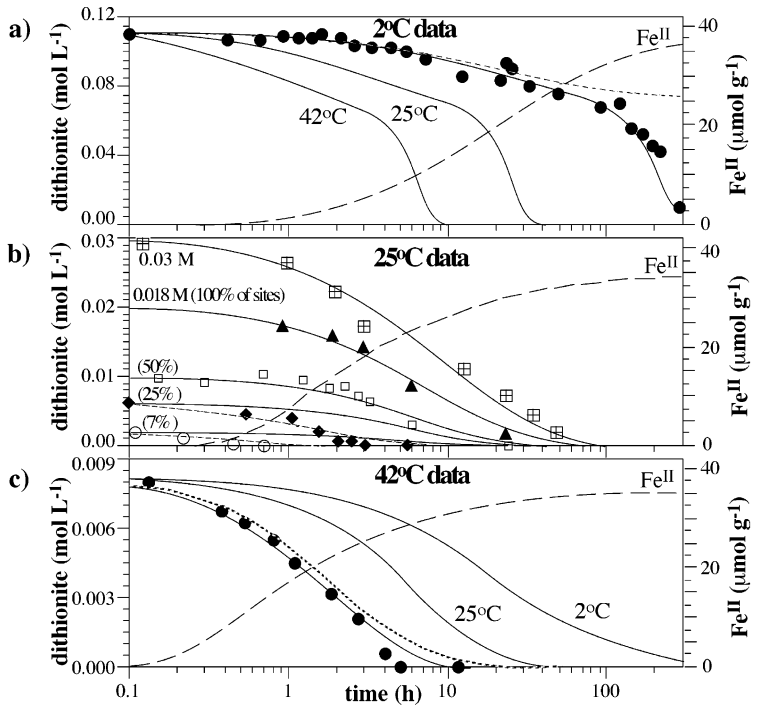

FIGURE 1. Batch reduction of sediment #1 using (a) 0.11 mol L^{-1} dithionite at 2 °C; (b) varied dithionite concentrations at 25 °C: (0.002 mol L^{-1} (○), 0.0045 mol L^{-1} (◆), 0.009 mol L^{-1} (□), 0.018 mol L^{-1} (▲), 0.03 mol L^{-1} (open box with cross); (c) 0.008 mol L^{-1} dithionite at 42 °C. Lines are simulations of dithionite with reduction and disproportionation reactions (solid and dotted lines in b), dithionite with reduction only (dotted lines in a and c), and ferrous iron produced (dashed lines).

unaccounted for in these amorphous and crystalline iron oxide extractions. Because structural iron in smectite clays can be reduced by dithionite,[30] there may be some contribution from clays (likely varies with the sedimentary environment). During reduction, the increase in Fe^{II} phases for sediments 1, 2, and 4 (80, 28, 20 μmol g^{-1}) was greater than the decrease in Fe^{III} oxides (60, 20, 9 μmol g^{-1}), suggesting additional Fe^{III} phases contributing to predominantly adsorbed Fe^{II}, when reduced. Dithionite treatment also resulted in an increase in surface area by EGME (untreated 31, reduced 43 m^2 g^{-1}), possibly by removal of some iron oxides from clay surfaces.

Subsequent oxidation of dithionite-reduced sediment (Table 1) resulted in the disappearance of the adsorbed Fe^{II}, some decrease in siderite/FeS, and an increase in dominantly amorphous Fe^{III} oxides. The apparent slow oxidation of siderite/FeS may correspond to the oxidation resistant fraction (described in the next section). Quantifying oxygen consumption during oxidation of the reduced sediment in columns was used to determine the total "reductive capacity" of the sediment and compared with these iron phase changes in a following section.

Sediment Reduction Rate. The rate of iron reduction and reaction order was quantified in batch experiments from the rate of disappearance of dithionite at different relative dithionite/sediment proportions and different temperatures (Figure 1). Iron reduction was visually observed from the sediment color change from tan to gray (within 10 h), or black (FeS) at high dithionite concentration. Because dithionite is consumed by both iron reduction (~4-h half-life) and disproportionation (~27-h half-life), excess dithionite is needed to fully reduce sediment. An experiment at 0.1 mol L^{-1} dithionite (at 2 °C) shows consumption predominantly by iron reduction for the first 100 h (Figure 1a) followed by the increased consumption by disproportionation after 100 h.

The average reduction half-life of the silty gravel (sediment 1, Figure 1) in batch systems assuming a third-order reduction reaction, was 3.3 ± 0.7 h at 25 °C. Reduction and disproportionation rates were determined from simulations of time-dependent dithionite consumption from reduction (reactions 1 and 2) and disproportionation (reaction 3). In general, simulations assuming a third-order reduction of Fe^{III} phases and first-order disproportionation of dithionite reactions match the observed data. Therefore, the natural sediment could be modeled as a single reductive dissolution reaction even though extraction data (previous section) indicated that multiple Fe^{III} phases were being reduced and one or more Fe^{II} phases were produced. Simulation at high dithionite concentration (Figure 1a, lines) matches the two slopes (i.e., two reactions) of the data. A simulation without disproportionation (dotted line) shows the fraction of dithionite used for iron reduction only. Simulations of the low dithionite concentration experiment (Figure 1c) with and without disproportionation are nearly the same because almost no dithionite was used for disproportionation within 10 h. The simulated increase in ferrous iron reaches 50% of total iron by 22 h (2 °C, Figure 1a) and by 0.8 h (42 °C, Figure 1c).

Experiments varying the dithionite/sediment proportions showed that iron phases present were reduced at different rates (Figure 1b). In experiments with a large amount of dithionite relative to reducible iron (170, 100, 50% dithionite/reducible iron, Figure 1b solid lines) dithionite consumption was well simulated by a single reduction rate. However, when the dithionite mass was only 25%, or 7% of the reducible iron (diamonds, circles, Figure 1b), a 5 to 15 times faster reduction rate is needed to match the data (dashed lines). These faster rates may correspond to faster dissolution/reduction of amorphous Fe^{III} phases. If correct, this would support our first hypothesis that several iron phases are being dissolved by the dithionite treatment.

The iron reductive dissolution half-life (3.3 h) for dithionite treatment of natural sediments in this study is similar to or faster than the reduction of surface phases by other complexes, despite differing mechanisms. The reduction reaction half-life of Fe^{III}(hydr)oxide (pure phase) by oxalate at pH 3

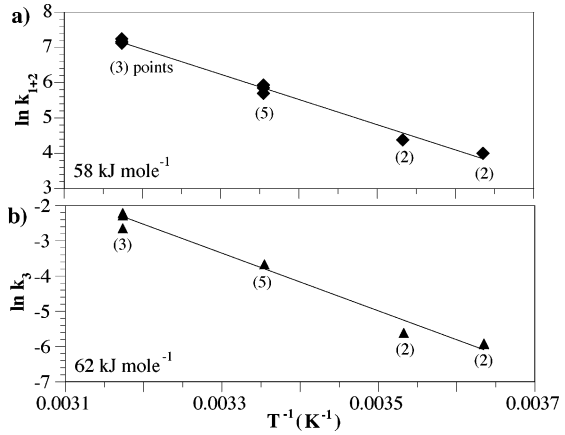

FIGURE 2. Batch experiment temperature dependence of (a) sediment reduction rate, and (b) dithionite disproportionation rate.

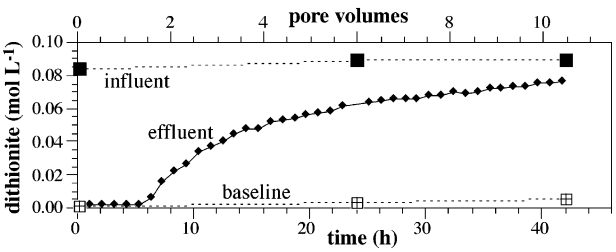

FIGURE 3. Reduction of sediment #1 in a 1-D column with a residence time of 4.0 h.

is 0.6−1.1 h (*40*), whereas the reduction half-life of ferrihydrite-coating sand by $Co^{II}EDTA$ at pH 7.0 is 5.0−53 h (*41*). The reduction half-life of a natural sediment (0.14% iron of poorly crystalline goethite, hematite, and ferroxyhite) by $Co^{II}EDTA$ at pH 6.5 is 49 h (*42*). The production of significant Fe^{II} and subsequent adsorption will slow additional reductive dissolution, as observed during microbial iron reduction (*43*, *44*).

Temperature Studies. The batch sediment reduction experiments conducted at temperatures from 2 to 42 °C provided an understanding of the rate-limiting step for reduction and disproportionation. Dithionite consumption increased with temperature (Figure 1), although simulations were needed to quantify the increases with temperature of both the iron reduction half-life (2.3 times per 10 °C) and disproportionation half-life (3.0 times per 10 °C). The activation energy for reduction (Figure 2a, 58 kJ mol^{-1}) indicated chemical control. The reduction of vinyl chloride by Fe^0 was also chemically controlled (*45*) (activation energy of 42 kJ mol^{-1}), but the reduction of carbon tetrachloride by Fe^0 was likely diffusion controlled (low activation energy (*46*)). Disproportionation, an aqueous chemical reaction, was chemically controlled (Figure 2b, 62 kJ mol^{-1}), as expected.

Reductive Capacity and Reduction Rate in Sediment Columns. Because this chemical injection technology is being used in groundwater wells, accurate sediment reduction mass and rates at high field sediment/water ratios and during advective flow are needed. Although the sediment reduction rate in batch systems is chemically controlled, additional mass transfer limitations such as intraparticle diffusion may additionally slow the observed reduction rate during advective flow. Toward that end, mass balance of aqueous species was conducted during reduction and oxidation in 1-D columns (Table 2) to quantify the reductive capacity and reduction rate.

In flow experiments during reduction (4-h residence time, Figure 3), 42% of the injected sodium dithionite is consumed by iron reduction and 9.5% is consumbed by disproportionation. After initial breakthrough, the aqueous dithionite concentration continues to increase as less is consumed by iron reduction. The mass of reduced iron was calculated from the total dithionite mass loss minus the consumption by disproportionation (Table 2). The disproportionation loss was calculated based on the residence time in columns and the aqueous disproportionation rate (*47*). The mass of Fe^{II} phases in reduced sediment was additionally calculated from oxygen consumption during sediment oxidation by air-saturated water in columns (Figure 4, Table 2). Oxygen consumption behavior was dependent on the oxygen-reduced sediment contact time. With a long residence time (60 h; Figure 4a), equilibrium-like breakthrough behavior is observed, but with considerably shorter residence times (0.6 h, Figure 4b), multiple slopes of the breakthrough shape were observed. These multiple breakthrough curve shapes during oxidation are indicative of more than one reduced surface iron phase being oxidized at different rates. This may correspond with the adsorbed Fe^{II} and a lesser amount of siderite/FeS shown with iron extraction data. Simulation of oxygen breakthrough is possible with a single oxidation reaction at long residence time, but at least two oxidation reactions (different oxidation rates) are needed to approximate the oxygen breakthrough curve shape at short residence times (line in Figure 4b).

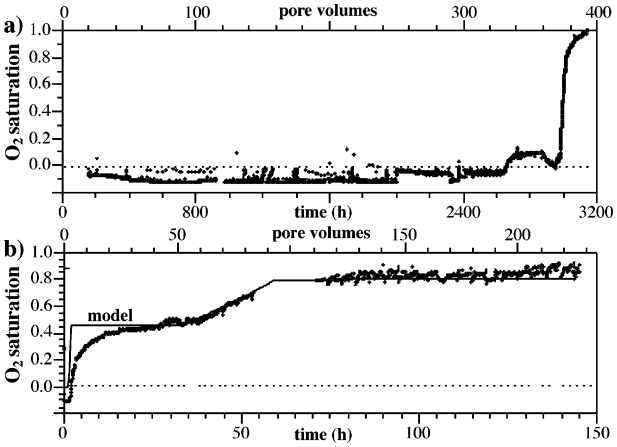

FIGURE 4. Oxidation of sediment #1 in columns with oxygen-saturated water at differing residence times (a) 60 h, and (b) 0.6 h. Simulation shown (line in b) uses two oxidation reactions.

The calculated mass of iron reduced in reduction experiments was roughly comparable to the mass of iron oxidized (within 20%, Table 2), although Fe^{II} oxidized values were generally lower. Because some reduced phases were slow to oxidize, a small percent (10−20%) of the reduced iron was not oxidized within 100- to 400-h oxidation experiments reported in Table 2 (Figure 4b, final value 90% O_2 saturation after 150 h). Reductive capacity calculated from the oxidation experiments are considered more accurate because only oxygen consumption data were needed, whereas reduction capacity from the mass of iron reduced required both dithionite consumption data and calculation of the disproportionation mass loss. The reductive capacity was reproducible for the same dithionite treatment (±10%, excluding experiments D−G, different pH buffer, Table 2). Iron extraction data (Table 1) show that sorbed Fe^{II} and siderite/FeS account for most of the reductive capacity for sediments 1, 2, and 4, but only a portion of sediment 3. As stated earlier, chemical extractions do not account for all iron phase changes occurring during reduction.

Although a portion of the reductive capacity observed in sediment columns could be residual dithionite, evidence indicates that this is likely small. First, disproportionation in aqueous solution (reaction 3) will react nearly all of the

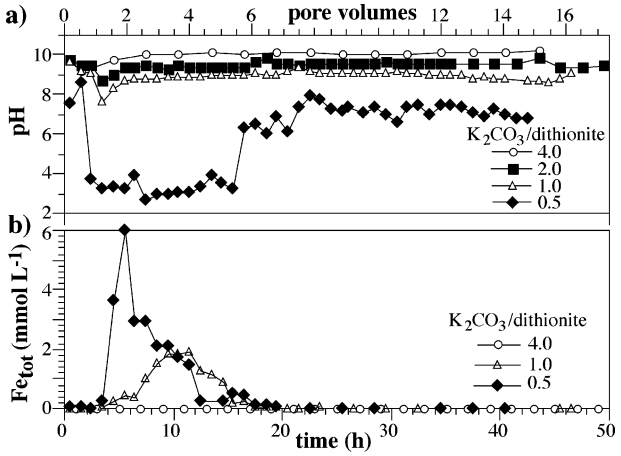

FIGURE 5. Column reduction of sediment #1 at different pH buffer (K_2CO_3) concentrations relative to sodium dithionite, showing the effluent (a) pH, and (b) aqueous iron.

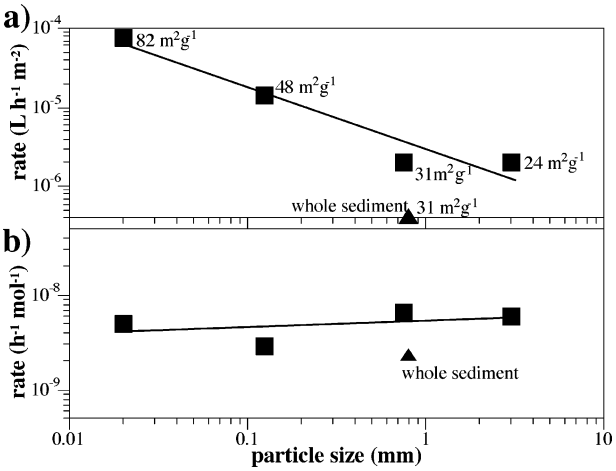

FIGURE 6. TCE dechlorination rate for different particle size fractions of sediment #1 normalized by (a) total surface area, and (b) reducible iron content.

dithionite within a week, so there should be no residual dithionite in aqueous solution. Second, dithionite sorption is small, based on conservative breakthrough of dithionite injected into a previously reduced sediment (i.e., retardation factor of 1.05, data not shown). Thus, there appears to be no mechanism to hold dithionite at the sediment surface.

The iron reduction rates in columns (expressed as half-lives, Table 2) were all slower than in batch experiments, suggesting some diffusional limitations. For the silty gravel (#1), column reductions had an average half-life of 8.0 ± 2.5 h (Table 2), compared with 3.3 ± 0.7 h in batch (Figures 1 and 2) at 25 °C. The sediment oxidation rate observed for the natural sediments in this study (~12-min half-life, Figure 4b, pH 8) were an order of magnitude slower than those observed for aqueous Fe^{2+}. The rate of aqueous Fe^{2+} oxidation by dissolved oxygen at pH 7 has been observed with a 4- to 83-min half-life (*48*, *49*) and a 3- to 50-s half-life at pH 8.

pH Control During Reduction. A total of four moles of H^+ per mole of dithionite is generated during iron reduction (reactions 1 and 2), so a K_2CO_3/dithionite ratio of 4 is needed to maintain pH. The use of less pH buffer was investigated (experiments D−G, Table 2) to determine the influence of sediment buffering. With less pH buffer, a low pH front resulted which mobilized some iron and reduced less iron (iron reduction rate is slower at lower pH). In all column experiments, 0.09 mol L^{-1} sodium dithionite was injected, with an influent pH of 10.5 (Figure 5a). With a high concentration of the pH buffer (CO_3/dith. = 4 or 2), the effluent pH was 9.5 to 10.0, but with less buffer, the pH dropped significantly (CO_3/dith. = 1, pH = 7.7; CO_3/dith. = 0.5, pH = 2.3). As expected, iron leaching increased at low pH. A total of 0.21% of the iron in the column was mobilized at pH 9.5 (CO_3/dith. = 4), 0.94% at pH 7.7 (CO_3/dith. = 1), and 3.3% at pH 2.3 (CO_3/dith. = 0.5). The practice of injecting aqueous Fe^{II} species at the field scale at low pH has been observed to be ineffective due to this iron mobility (*50*).

Although the pH decrease and iron mobility appeared minor with less pH buffer, there was significant impact on reductive capacity and contaminant reactivity. Sediments reduced with high buffer (CO_3/dith. = 4) achieved high reduction (159 μmol g^{-1}), but with less buffer, significantly less iron was reduced (79, 58, and 41 μmol g^{-1} for CO_3/dith. = 3, 2, and 0.5, respectively, Table 2, experiments E−G). The resulting TCE degradation half-life indicated even worse performance, as described in the following section. While sediment buffering can be significant over long time scales, these results indicate that there would be little buffering capacity in field-scale dithionite injection experiments because of the short residence times.

Reduced Sediment Reactivity with TCE. To quantify which ferrous surface phase was redox reactive, the TCE dechlorination rate of dithionite-reduced sediment (#1) was compared in: (a) fully and partially reduced sediment, (b) chemically altered sediment, and (c) physically separated fractions of the same sediment. Experiments in partially reduced sediment (previous section) quantified the influence of mass of ferrous iron on the TCE degradation rate. The chemically altered fractions (sequential chemical extractions) were used to remove potentially reactive surface phases. TCE is abiotically transformed to chloroacetylene then acetylene by reductive elimination (*15*, *51*). TCE dechlorination is controlled by surface ferrous iron, given that dithionite and aqueous Fe^{2+} do not dechlorinate TCE. The rate of TCE transformation to acetylene is used as a measurement of the mass of surface ferrous iron.

The TCE degradation half-life was highly dependent on the reductive capacity. Fully reduced sediment (reductive capacity 159 μmol g^{-1}, Table 2) had a 1.2- to 5.4-h TCE degradation half-life (*15*), whereas partially reduced sediment (described in previous section; 58 and 41 μmol g^{-1}, experiments E and F, Table 2) had 200-h and 1400-h half-lives, respectively.

The rate of TCE transformation was 10 times faster for finer grain size fractions (2.7-h half-life for <30 μm size; 28-h half-life for 2−4 mm size), and the TCE transformation rate per unit surface area was still a function of particle size (<30 μm was 37 times faster than 2−4 mm, Figure 6a). The <30 μm size fraction (82% clay) dominated TCE reactivity. These rates (av 1.9 × 10^{-5} L h^{-1} m^{-2}) were an order of magnitude slower than those of zerovalent iron (av 2.8 × 10^{-4} L h^{-1} m^{-2} (*52*)), although normalizing for the total surface area underestimates the reactivity of the ferrous iron surface phases, which are only a fraction of the total surface area. The TCE degradation rate per mole of reduced Fe^{II} (Figure 6b) showed no size fraction trend and had less variability (2.3 to 6.6 × 10^{-9} h^{-1} mol^{-1}), so may represent reactivity better for a heterogeneous surface.

Chemical extractions used to remove selected iron phases before or after dithionite treatment confirmed that adsorbed Fe^{II} dominated TCE reactivity. It should be stated that chemical extractions remove most of the surface phase(s) stated, but there are limitations to this approach. The importance of adsorbed Fe^{II} for dechlorination is shown by comparing the 23-h TCE degradation half-life for reduced sediment (Figure 7a, squares), with the 533-h half-life obtained when adsorbed Fe^{II} was removed after reduction (triangles, 1 M $CaCl_2$ extraction after reduction). In a separate

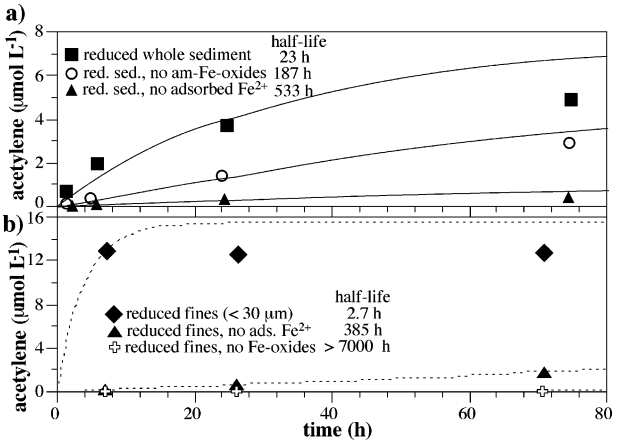

FIGURE 7. TCE abiotic reduction to acetylene for (a) whole sediment #1, and (b) <30-μm size fraction of sediment #1. Chemical extractions were used to remove iron phases before or after chemical reduction of sediment.

experiment, amorphous Fe^{III} oxides were removed before dithionite reduction. The TCE transformation rate (187-h half-life, circles, Figure 7a) decreased relative to reduced sediment, consistent with a decrease in the available Fe^{II} reductant. Both amorphous and crystalline Fe^{III} oxides decrease upon dithionite reduction and contribute to adsorbed Fe^{II} (Table 1).

The <30 μm fraction of the sediment (82% clay) was subjected to sequential chemical extractions to address the role of structural ferrous iron on TCE reactivity. The reduced <30 μm fraction with no extractions quickly reduced TCE (2.67-h half-life; Figure 7b, diamonds). TCE was transformed 14 times slower (385-h half-life) when adsorbed Fe^{2+} was removed after reduction (triangles), again indicating adsorbed Fe^{2+} was the main electron donor, but some reactivity remained. Removal of amorphous and crystalline iron oxides (DCB extraction) first before dithionite reduction resulted in the complete lack of TCE dechlorination. These results imply that any reduced structural iron in the 82% clay present in this <30 μm size fraction had little reactivity. A similar conclusion was reached in a study on chromate reduction by natural sediments (adsorbed Fe^{II} dominated reactivity) (*53*), but was in contrast to another study in which the reduction of nitroaromatics was caused both by adsorbed iron on edge surfaces of clays as well as structural iron in the 2:1 smectite clays (*54*).

Application to Field Scale Reduction. The chemical reduction of aquifer sediments is a viable technology for groundwater remediation of contaminants because a sufficient mass of immobile reduced iron phases is created over a large volume that should lpast decades (i.e., hundreds of pore volumes, Figure 4). Reduction rates in this study (Table 2) show that dithionite reduction of sediments requires hours to tens of hours, which allows for sufficient time for field-scale injections to treat sediments in a zone 40−50 ft in diameter. Field-scale permeable reduced zones implemented at several sites (*13*, *55*) have achieved the reductive capacity observed in these laboratory experiments, which indicates that the influence of physical and chemical spatial heterogeneities appears to be minor. At a Cr-contaminated aquifer in eastern Washington, coring into the reduced zone showed a reductive capacity of 10.6 ± 6.6 μmol g^{-1} (n = 9), whereas laboratory experiments (sediment 4, Table 2) averaged 11.2 ± 7.4 μmol g^{-1} (n = 16).

Although well-designed redox-reactive in situ barriers function in homogeneous field systems, physical heterogeneities (high permeability channels) affect all in situ barriers. With greater lateral extent of high permeability channels, thin (2−4 ft wide) zerovalent iron barriers will suffer premature breakthrough of contaminants due to insufficient residence time for degradation (*29*). While this dithionite treatment creates significantly wider zones and will perform better with the same scale of heterogeneity, this technology is also dependent on spatial variability of the reducible iron content being sufficiently large at all locations. Large-scale high flow/low iron content deposits could prematurely oxidize a section of a barrier. The spatial variability observed in the reducible iron content varied from uniform for a fluvial deposit (sediment 3, 520 ± 20 μmol g^{-1}, n = 11) to highly variable for a glacial deposit (sediment 1, 159 ± 45.3 μmol g^{-1}, n = 26). Other studies have shown that chemical heterogeneities (*42*) and physical/chemical heterogeneities (*56*, *57*) have other effects that highly influence predicted reactive transport behavior. While the laboratory experiments presented here and field scale observations demonstrate that natural sediments at great depth can be chemically reduced to act as a permeable reduction barrier, this technology is more influenced by aquifer geochemical conditions and perhaps less influenced by hydraulic spatial variability relative to installed permeable barrier systems.

Acknowledgments

Financial support for this project was provided by the U.S. Department of Energy, Natural and Accelerated Bioremediation Research (DOE/NABIR) program, U.S. Department of Defense, and the Strategic Environmental Research and Development Program (SERDP). The Pacific Northwest National Laboratory is operated by Battelle Memorial Institute for the U.S. Department of Energy under Contract DE-AC06-76RLO1830.

Literature Cited

(1) McNab, J. W. W.; Ruiz, R.; Reinhard, M. *Environ. Sci. Technol.* **2000**, *34*, 149−153.
(2) Eary, L. E.; Rai, D. *Environ. Sci. Technol.* **1988**, *22*, 972−977.
(3) Farrell, J.; Wang, J.; O'Day, P.; Conklin, M. *Environ. Sci. Technol.* **2001**, *35*, 2026−2032.
(4) Loyaux-Lawniczak, S.; Lecomte, P.; Ehrhardt, J. *Environ. Sci. Technol.* **2001**, *35*, 1350−1357.
(5) Morrison, S.; Metzler, D.; Carpenter, C. *Environ. Sci. Technol.* **2001**, *2001*, 385−390.
(6) Nzegung, V. A.; Castillo, R. M.; Gates, W. P.; Mills, G. L. *Environ. Sci. Technol.* **2001**, *35*, 2244−2251.
(7) Hageman, K. J.; Istok, J. D.; Field, J. A.; Buschek, T. E.; Semprini, L. *Environ. Sci. Technol.* **2001**, *35*, 1729−1735.
(8) Agrawal, A.; Tratnyek, P. *Environ. Sci. Technol.* **1996**, *30*, 153−160.
(9) Alowitz, M. J.; Scherer, M. M. *Environ. Sci. Technol.* **2002**, *36*, 299−306.
(10) Devlin, J. F.; Muller, D. *Environ. Sci. Technol.* **1999**, *33*, 1021−1027.
(11) Waybrant, K. R.; Blowes, D. W.; Ptacek, C. J. *Environ. Sci. Technol.* **1998**, *32*, 1972−1979.
(12) Appleton, E. L. *Environ. Sci. Technol.* **1996**, *30*, 536A−539A.
(13) Fruchter, J.; Cole, C.; Williams, M.; Vermeul, V.; Amonette, J.; Szecsody, J.; Istok, J.; Humphrey, M. *Ground Water Monit. Rev.* **2000**, *1*, 66−77.
(14) Szecsody, J.; Fruchter, J.; McKinley, M.; Gilmore, T. *Feasibility of In Situ Redox Manipulation for RDX Remediation in Pantex Sediments*; Pacific Northwest National Laboratories: Richland, Wa, 2001.
(15) Szecsody, J.; Williams, M.; Fruchter, J.; Vermeul, V.; Evans, J. C. In *Chemical Oxidation and Reactive Barriers*; Wickramanayake, G., Ed.; Battelle Press: Columbus, OH, 2000; Vol. Remediation of Chlorinated and Recalcitrant Compounds, pp 369−376.
(16) Rodriguez, E.; Amonette, J.; Divanfard, H.; Marquez, J. In *Remediation of Chlorinated and Recalcitrant Compounds*; Wickramanayake, G. B., Hinchee, R. E., Eds.; Battelle Press: Columbus, OH, 1998; Vol. C1−5, pp 335−340.
(17) Cervini-Silva, J.; Larson, R. A.; Wu, J.; Stucki, J. W. *Environ. Sci. Technol.* **2001**, *35*, 805−809.
(18) Amonette, J.; Workman, D.; Kennedy, D.; Fruchter, J.; Gorby, Y. *Environ. Sci. Technol.* **2000**, *34*, 4606−4613.

(19) Rodriguez, E.; Amonette, J.; Divanfard, H.; Marquez, J. In *Environmental Molecular Sciences Symposia and First Users Meeting*; Pacific Northwest National Laboratory: Richland, WA, 1999; pp 41−42.
(20) Balko, B. A.; Tratnyek, P. G. *J. Phys. Chem. B* **1998**, *102*, 1459−1465.
(21) Scherer, M.; Balko, B.; Tratnyek, P. In *ACS Symposium Series #715*; Sparks, D. L., Grundl, T., Eds.; American Chemical Society: Washington, DC, 1999; pp 1−22.
(22) Wehrli, B. In *Aquatic Chemical Kinetics*; Stumm, W., Ed.; John Wiley and Sons: New York, 1992; pp 311−337.
(23) Hung, H.; Hoffman, M. R. *Environ. Sci. Technol.* **1998**, *32*, 3011−3016.
(24) Farrell, J.; Kason, M.; Melitas, N.; Li, T. *Environ. Sci. Technol.* **2000**, *34*, 514−521.
(25) Sivavec, T.; Mackenzie, P.; Horney, D.; Baghel, S. *Redox-Active Media for Permeable Reactive Barriers*; General Electric Research and Development Center: , 1996.
(26) Seaman, J. C.; Bertsch, P. M.; Schwallie, L. *Environ. Sci. Technol.* **1999**, *33*, 938−944.
(27) Loyaux-Lawniczak, S.; Refait, P.; Ehrhardt, J. J.; Lacomte, P.; Genin, J. R. *Environ. Sci. Technol.* **2000**, *34*, 438−443.
(28) Szecsody, J.; Williams, M.; Fruchter, J.; Vermeul, V.; Evans, J. In *Chemical Oxidation and Reactive Barriers*; Wickramanayake, G., Ed.; Battelle Press: Columbus, OH, 2000; Vol. C2−6, pp 377−384.
(29) Eykholt, G.; Elder, C.; Benson, C. *J. Hazard. Mater.* **1999**, *68*, 73−96.
(30) Stucki, J. W.; Golden, D. C.; Roth, C. B. *Clays Clay Miner.* **1984**, *32*, 191−197.
(31) Amonette, J.; Templeton, J.; Speed, R.; Zipperer, J. Chemistry of Dithionite Ion in Aqueous Suspensions of Clay Minerals. In *SSSA Meetings*; Soil Science Society of America: Minneapolis, MN, 1992; pp 1−16.
(32) Buerge, I. J.; Hug, S. J. *Environ. Sci. Technol.* **1997**, *31*, 1426−1432.
(33) Heron, G.; Crouzet, C.; Bourg, A. C.; Christensen, T. H. *Environ. Sci. Technol.* **1994**, *28*, 1698−1705.
(34) Chao, T. T.; Zhou, L. *Soil Sci. Soc. Am. J.* **1983**, *47*, 225−232.
(35) Gibbs, C. R. *Anal. Chem.* **1976**, *48*, 1197−1200.
(36) Szecsody, J. E.; Zachara, J. M.; Chilakapati, A.; Jardine, P. M.; Ferrency, A. S. *J. Hydrol.* **1998**, *209*, 112−136.
(37) Lee, W.; Batchelor, B. *Environ. Sci. Technol.* **2003**, *37*, 535−541.
(38) Hindmarsh, A. C. In *Scientific Computing*; Stepleman, R. S., Ed.; North-Holland: New York, 1983; pp 55−64.
(39) Chilakapati, A.; Williams, M.; Yabusaki, S.; Cole, C. *Environ. Sci. Technol.* **2000**, *34*, 5215−5221.
(40) Suter, D.; Banwart, S.; Stumm, W. *Langmuir* **1991**, *7*, 809−813.
(41) Brooks, S.; Taylor, D.; Jardine, P. *Geochim. Cosmochim. Acta* **1996**, *60*, 1899−1908.
(42) Szecsody, J. E.; Chilakapati, A.; Zachara, J. M.; Garvin, A. L. *Water Resour. Res.* **1998**, *34*, 2501−2514.
(43) Liu, C.; Szecsody, J.; Zachara, J.; Ball, W. *Adv. Water Resour.* **2000**, *23*.
(44) Roden, E. E.; Zachara, J. M. *Environ. Sci. Technol.* **1996**, *30*, 1618−1628.
(45) Deng, B.; Burris, D. R.; Campbell, T. J. *Environ. Sci. Technol.* **1999**, *33*, 2651−2656.
(46) Matheson, L.; Tratnyek, P. *Environ. Sci. Technol.* **1994**, *28*, 2045−2053.
(47) Amonette, J. In *Electrochemistry of Clays*; Fitch, A., Ed.; Clay Minerals Society: 2000; Vol. CMS Workshop Lectures.
(48) Roekens, E.; van Grieken, R. *Mar. Chem.* **1983**, *13*, 195−202.
(49) Sung, W.; Morgan, J. *Environ. Sci. Technol.* **1980**, *14*, 561−568.
(50) Seaman, J.; Bertsch, P.; Korom, S.; Miller, W. *Ground Water* **1996**, *34*, 778−783.
(51) Roberts, A. L.; Totten, L. A.; Arnold, W. A.; Burris, D. R.; Campbell, T. J. *Environ. Sci. Technol.* **1996**, *30*, 2654−2659.
(52) Trantnyek, P.; Scherer, M. M.; Johnson, T.; Matheson, L. In *Chemical Degradation Methods for Wastes and Pollutants: Environmental and Industrial Applications*; Tarr, M. A., Ed.; Marcel Dekker: New York, 2003.
(53) Buerge, I. J.; Hug, S. J. *Environ. Sci. Technol.* **1999**, *33*, 4285−4291.
(54) Hofstetter, T. B.; Schwarzenbach, R. P.; Handerlein, S. B. *Environ. Sci. Technol.* **2003**, *37*, 519−528.
(55) Vermeul, V.; Williams, M.; Szecsody, J.; Fruchter, J.; Cole, C.; Amonette, J. In *Groundwater Remediation of Trace Metals*; Winkle, G., Ed.; Academic Press: New York, 2002.
(56) Bosma, W.; van der Zee, S. *Transp. Porous Media* **1995**, *18*, 181−198.
(57) Rubin, Y. *Water Resour. Res.* **1995**, *31*, 2461−2468.

Received for review July 13, 2003. Revised manuscript received June 16, 2004. Accepted June 21, 2004.

ES034756K